Journal of Power Sources 255 (2014) 325–334

Contents lists available at ScienceDirect

Journal of Power Sources

journal homepage: www.elsevier.com/locate/jpowsour

Anion exchange membrane prepared from simultaneous polymerization and quaternization of 4-vinyl pyridine for non-aqueous vanadium redox flow battery applications

Sandip Maurya, Sung-Hee Shin, Ki-Won Sung, Seung-Hyeon Moon*

School of Environmental Science and Engineering, Gwangju Institute of Science and Technology (GIST), 123 Cheomdan-gwagiro, Buk-gu, Gwangju 500-712, Republic of Korea

HIGHLIGHTS

- AEMs were prepared by a simple, single step and environmentally friendly process.
- Anion exchange membrane synthesis by simultaneous polymerization and quaternization.
- Quaternization with bifunctional agent introduces crosslinking.
- The permeability of charged species was suppressed due to the crosslinking.
- The maximum energy efficiency of 87.7% was obtained in cyclic operation.

GRAPHICAL ABSTRACT

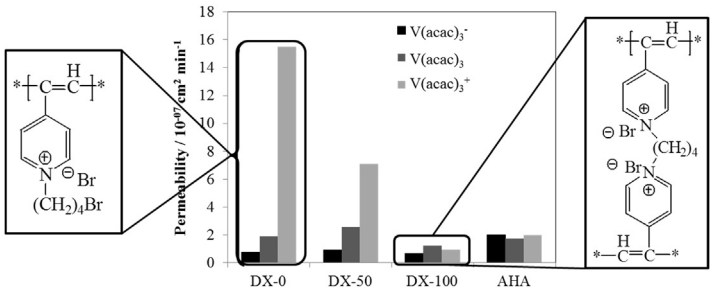

ARTICLE INFO

Article history:
Received 15 November 2013
Received in revised form
7 January 2014
Accepted 9 January 2014
Available online 18 January 2014

Keywords:
Anion exchange membrane
Simultaneous polymerization and quaternization
Crosslinking
Mechanical stability
Non-aqueous vanadium redox flow battery

ABSTRACT

A simple, single step and environmentally friendly process is developed for the synthesis of anion exchange membrane (AEM) by simultaneous polymerization and quaternization, unlike the conventional membrane synthesis which consists of separate polymerization and quaternization step. The membrane synthesis is carried out by dissolving polyvinyl chloride (PVC) in cyclohexanone along with 4-vinyl pyridine (4VP) and 1,4-dibromobutane (DBB) in the presence of thermal initiator benzoyl peroxide, followed by film casting to get thin and flexible AEMs. The membrane properties such as ion exchange capacity, ionic conductivity and swelling behaviour are tuned by varying the degree of crosslinking. These AEMs exhibit low vanadium permeability, while retaining good dimensional and chemical stability in an electrolyte solution, making them appropriate candidates for non-aqueous vanadium acetylacetonate redox flow battery (VRFB) applications. The optimized membrane displays ion exchange capacity and ionic conductivity of 2.0 mequiv g^{-1} and 0.105 mS cm^{-1}, respectively, whereas the efficiency of 91.7%, 95.7% and 87.7% for coulombic, voltage and energy parameter in non-aqueous VRFB, respectively. This study reveals that the non-aqueous VRFB performance is greatly influenced by membrane properties; therefore the optimal control over the membrane properties is advantageous for the improved performance.

© 2014 Elsevier B.V. All rights reserved.

1. Introduction

Vanadium redox flow battery was conceptualized in 1985 [1,2] and further developed by Skyllas-Kazacos and co-workers [3]. It

* Corresponding author. Tel.: +82 62 715 2435; fax: +82 62 715 2434.
E-mail address: shmoon@gist.ac.kr (S.-H. Moon).

0378-7753/$ – see front matter © 2014 Elsevier B.V. All rights reserved.
http://dx.doi.org/10.1016/j.jpowsour.2014.01.047

is a promising electrochemical energy storage system for the electrical power generating systems due to its attractive features such as high power density, various loading levels and considerable energy efficiency [4]. Electrical energy is generated by a redox reaction of V^{+2}/V^{+3} and VO^{2+}/VO_2^+ redox couples in sulfuric acid as negative and positive electrolyte respectively that is separated by an ion exchange membrane [4]. The presence of dissimilar redox couple makes vanadium redox flow battery significantly prone to the active species crossover resulting in energy and capacity losses, which require periodic electrolyte rebalancing [5]. Moreover, the aqueous electrolyte solution limits the coulombic efficiency, capacity, potential window and operating temperature range [6].

Despite of several advancements in membrane separators and electrodes for vanadium redox flow batteries, the concern over capacity loss, operating potential and temperature are remained unsolved [7–12]. In a novel approach, non-aqueous RFBs were introduced with organic solvents and compatible redox couples and supporting electrolytes instead of vanadyl sulfate-sulfuric acid [13,14]. Various non-aqueous redox couples such as modified anthraquinone–lithium [15], uranium β-diketonates, iron tris(bipyridyl) perchlorate [14] and acetylacetonates of ruthenium [14], vanadium [16], chromium [17] and manganese [18] have been studied. Non-aqueous electrolytes enable cell operation at higher potential compared to aqueous electrolyte and thus lead to higher energy density and energy efficiency [15]. Moreover, the charged metal redox couple reverts to the same species on discharge by a single electron disproportionation which minimizes the need for periodical electrolyte regeneration [16]. Among the tested metal redox couples, vanadium acetylacetonate has shown reasonably good reversibility, open circuit voltage (OCV, ~2.2 V) and coulombic efficiency (~85–90%) [19]. Reports on the use of the porous glass, porous polymeric membrane and commercial AEMs are available for non-aqueous RFBs [13,16,20]. Specifically, commercial Neosepta AHA (Astom, Japan) and AMI-7001 (membrane international Inc., USA) membranes have originally been developed for the water based applications such as desalination of brackish and sea water, electrodialysis and treatment of industrial waste water, and they have shown poor chemical and mechanical stability in organic electrolyte solutions [21]. Therefore, there is an enormous scope of research for battery separator/membrane suitable for non-aqueous applications [20].

AEMs with pyridinium group have shown excellent electrochemical properties and oxidative stability in aqueous vanadium redox flow batteries [22,23]. Hence, it is desirable to study the AEMs having pyridinium groups for good resilience in organic solvent, electrochemical properties and low crossover of vanadium complex species. Interestingly, two poly(4-vinyl pyridine) chains in AEM can be simply and effectively crosslinked by bifunctional dihaloalkane without altering the density of ion exchange groups, which lowers the crossover and hence the membrane becomes advantageous for any RFB application [24]. More importantly, most AEM synthesis requires a complex procedure and toxic reagents, which is highly objectionable at environmental perspective. Therefore, the purpose of this study is to prepare a pyridinium group containing AEM by a simple, efficient and environmentally friendly process for non-aqueous RFB applications.

Herein, simultaneous polymerization and quaternization method to prepare crosslinked AEMs is demonstrated. Unlike the conventional membrane synthesis, which consists of separate polymerization and quaternization step, a single step method for the membrane preparation is developed. An inter-polymer of poly(vinyl chloride)/poly(4-vinyl pyridine) is synthesized by a solution polymerization of 4-vinyl pyridine and at the same time quaternized using 1,4-dibromobutane. The non-aqueous VRFB single cell performances with synthesized membranes show that the developed membrane has performed much better than commercial Neosepta AHA delivered higher capacity and coulombic efficiency.

2. Experimental

2.1. Materials

Polyvinyl chloride (PVC, Mw: 35000 g $mole^{-1}$), 4-vinyl pyridine, 1,4-dibromobutane, benzoyl peroxide for the preparation of membranes, were procured from Sigma–Aldrich Co., USA. Reagents for non-aqueous vanadium redox flow battery, vanadium(III) acetylacetonate ($V(acac)_3$), tetraethylammonium tetrafluoroborate ($TEABF_4$) and anhydrous acetonitrile (CH_3CN) from Sigma–Aldrich were used. Mili-Q water (18 MΩ) was used for membrane characterization. All chemicals were analytical grade only and used without further purification.

2.2. Membrane preparation by a single step method

A single step process involving simultaneous polymerization and quaternization was carried out for synthesis of the AEM. The polymer solution was prepared by dissolving PVC in 15 ml of cyclohexanone. Then 2.0 g of 4-vinyl pyridine was added as a monomer and 1,4-dibromobutane (DBB) in varying molar ratio (as shown in Table 1) was added to the clear polymer solution. Then, thermal radical initiator BPO (0.05 g) was added for the polymerization of 4-vinyl pyridine. The reaction mixture was stirred and the temperature was raised to 65 °C and maintained until a viscous solution was obtained. To fabricate the AEM, the viscous solution was directly casted into a thin film by using doctors blade and then dried in an oven at 80 °C for 12 h. Dried membranes were peeled off from glass plate carefully and washed several times with methanol and deionized water to remove the unreacted chemicals. Membranes were further treated with 0.5 M NaCl and stored in the same solution. The schematic reaction mechanism of the entire process is shown in Fig. 1. The degree of crosslinking was theoretically estimated from the molar ratio of 4-vinyl pyridine and 1,4-dibromobutane and presented in Table 1.

2.3. Membrane characterization

The synthetic route was confirmed using a FT-IR spectrometer (JASCO 460 Plus, Japan), where dried thin film of membrane samples were examined in FT-IR mode. A total 16 scans were collected for each sample and background with spectral resolution of 4 cm^{-1} in ambient conditions. Morphologies of the membranes were observed by Scanning Electron Microscopy (SEM; Hitachi S-4700, Japan).

The ion exchange capacity (IEC) of the synthesized membranes was determined by equilibrating them in 1 M NaCl solution to exchange Cl^- form. The membranes were then washed with DI water

Table 1
The composition of P4VP-DBB membranes synthesized in this study.

Membrane code[a]	PVC (wt, g)	Molar ratio		BPO (wt%)	Crosslinking[b], %
		4VP	DBB		
DX-0	2	1	1	1	0
DX-25	2	1	0.87	1	25
DX-50	2	1	0.75	1	50
DX-75	2	1	0.63	1	75
DX-100	2	1	0.5	1	100

[a] Degree of crosslinking (DX).
[b] Theoretical estimation.

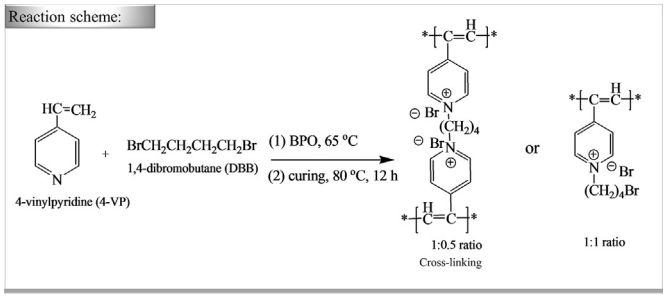

Fig. 1. A single step reaction for the preparation of membranes.

and further equilibrated with 1 M $NaNO_3$ where Cl^- was exchanged with NO_3^-. IEC was calculated from the amount of exchanged Cl^-, which in turn was determined by titration with 0.1 N $AgNO_3$ solution using K_2CrO_4 as an indicator. The following formula was used for calculation of IEC

$$\mathrm{IEC}\left(\mathrm{mequiv.\ g^{-1}}\right) = \frac{(v \times c)}{W_D} \quad (1)$$

where v, c and W_D are the volume of $AgNO_3$, the concentration of $AgNO_3$ and the weight of dried membrane, respectively.

The ionic conductivity of the membranes was determined by measuring electrical resistance them in 0.01 M $V(acac)_3$/0.1 M $TEABF_4/CH_3CN$ solution using two probe clip-cell. The ionic conductivity was calculated by the below equation:

$$\text{Ionic conductivity}\left(\mathrm{mS\ cm^{-1}}\right) = \frac{l}{R \times A} \quad (2)$$

where l, R, and A are the thickness of the membrane (cm), membrane area resistance ($\Omega\ cm^2$) and membrane area exposed to the electrode (cm^2).

Dimensional stability of prepared membranes was analyzed by swelling ratio. Prior to measurement, membranes were dried in oven at 50 °C for 24 h to remove the adsorbed moisture. It was immersed into 0.01 M $V(acac)_3$/0.1 M $TEABF_4/CH_3CN$ solution at a room temperature for 24 h and the dimensional changes of the membrane were measured in terms of swelling ratio in the thickness direction according to the following equation

$$\text{Swelling ratio}(\%) = \frac{l_s - l_d}{l_d} \times 100 \quad (3)$$

where l_d, and l_s are the thickness of the dry and swollen membrane respectively.

2.4. Vanadium permeability

To determine the permeability of the vanadium species, the membranes were sandwiched in the prototype flow cell as explained elsewhere [22,25]. The neutral 0.01 M $V(acac)_3$ solution was prepared by dissolving in anhydrous acetonitrile.0.1 M $TEABF_4$ was added as supporting electrolyte. Negatively charged and positively charged solutions were prepared by the electrochemical reduction and oxidation of the $V(acac)_3$ solution. The left reservoir was filled with 0.01 M of negative, neutral, or positively charged $V(acac)_3$ solution, and right was filled with only 0.1 M $TEABF_4$ solution. The two solutions were continuously flowed at 10 ml min^{-1} using a peristaltic pump at ambient condition. The effective area of the membrane was 3.14 cm^2 and the volume of each reservoir was 25 ml. Samples were collected periodically and treated with aquaregia in order to estimate vanadium concentration by ICP-OES (detailed procedure is explained in Supplementary information file). The permeability of vanadium species as a function of time were calculated from the below equation.

$$V\frac{dC_t}{dt} = A\frac{P}{L}(C_0 - C_t) \quad (4)$$

where, V is the volume of the reservoir, A, L and P are the membrane area, membrane thickness and the permeability of vanadium species. C_0 is the initial vanadium species concentration in left reservoir, and C_t is the vanadium species concentration in right reservoir at time t.

2.5. A non-aqueous vanadium acetylacetonate redox flow cell test

A flow type RFB cell modified from fuel cell was assembled with graphite felt (Nippon Graphite, GF-20-5F) as both electrodes ($5 \times 5 \times 0.5\ cm^3$). 40 mL of 0.01 M $V(acac)_3$/0.1 M $TEABF_4$ in CH_3CN was used as anolyte and catholyte solution. Peristaltic pump (Masterflex® L/S®, 7523-60, USA) was used to maintain the flow rate of 10 mL min^{-1} during the charge/discharge cycle and OCV curve measurement. Galvanostatic charge/discharge characteristic was observed in the voltage range of 1.7–2.5 V (SOC: 0.01–99.99) using battery cycler (Wonatech, WBCS3000K8, South Korea) at constant charge and discharge current density of 0.1 mA cm^{-2}. The coulombic efficiency (CE), voltage efficiency (VE) and energy efficiency (EE) of the cell were calculated from the following equations:

$$\mathrm{CE} = \frac{t_d}{t_c} \times 100\% \quad (5)$$

$$\mathrm{VE} = \frac{V_d}{V_c} \times 100\% \quad (6)$$

$$\mathrm{EE} = \mathrm{CE} \times VE \quad (7)$$

where t_d is the discharging time, t_c is the charging time, V_d is the average discharging voltage, and V_c is the average charging voltage.

3. Results and discussions

3.1. Synthesis of membrane

The synthesis of AEMs can be carried out from following different routes: (1) Polymerization of transformable functional group containing monomers which is followed by quaternization, (2) Chloromethylation of polymer followed by quaternization and (3) grafting of the anion exchange groups or their precursors by irradiation of polymer. These methods have disadvantages, such as use of toxic-carcinogenic organic compounds, long preparation time, complex process, disposal of large quantity of solvents and radiation hazards. Moreover, the commercial AEMs are prepared by the bulk polymerization of styrene/4-vinylbenzyl chloride (monomer) and divinylbenzene (crosslinking agent) followed by chloromethylation-quaternization or quaternization. The viscosity of the mixture of monomer solution is low which makes it difficult to cast into thin film, and also the reagents used for chloromethylation are proven carcinogens. In this study PVC and 4VP were used to increase viscosity of casting solution and to eliminate potential chloromethylation step from AEM preparation. PVC not only increases the viscosity of casting solution but also provides mechanical stability to the resultant membrane. The polymer system used here is based on poly(4-vinyl pyridine) (P4VP) which is an aromatic base with secondary nitrogen and able to undergo

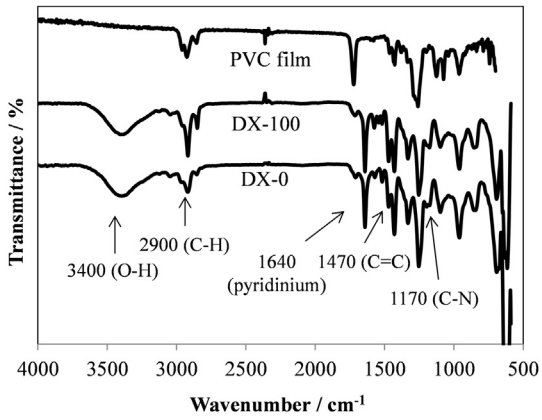

Fig. 2. ATR-IR spectra of (a) PVC film, (b) DX-0, and (c) DX-100.

quaternization without the need of chloromethylation. P4VP and quaternizing agent system allows the synthesis of the desired AEM with comparable pyridinium group density and variable crosslinking density. Fig. 1 shows a crosslinked-quaternized and only quaternized polymer network of the membranes. Beside the polymer system, the simultaneous polymerization and quaternization route was adopted for the synthesis of AEM. The applied synthetic route has successfully eliminated the need of separate step for chloromethylation and/or quaternization. As a result, the use of potentially carcinogenic chloromethyl methyl ether and bis-chloromethyl ether are avoided. Overall, this synthetic route for AEM preparation becomes shorter, cost effective and environmentally friendly.

The quaternization and polymerization reactions were confirmed by FT-IR analysis of membrane samples as shown in Fig. 2. The FT-IR spectra show the characteristic absorption bands at 1640 cm^{-1} which corresponds to the quaternized pyridine ring or pyridinium salt [26]. The broad and strong band at 3400 cm^{-1} corresponds to O—H stretching due to the hydrogen bond formation between quaternary functional group and the adsorbed water molecules, which is absent in the neat PVC film. Moreover, polymerization reaction is confirmed by the intense band at 1470 cm^{-1} for the aromatic C=C bond whereas the band at 1170 cm^{-1} is attributed to C—N stretching which itself is an evidence for successful quaternization and polymerization [20].

The cross section and surface morphology of the synthesized membranes is shown in Fig. 3. The cross section of DX-0 and DX-100 membranes (Fig. 3A and B) shows homogeneously distributed PVC and P4VP in membrane matrix without any macro-phase separation. The surface of the DX-100 membrane is smooth and homogeneous with some spherical polymer domains which indicate the excellent compatibility between the PVC and quaternized-crosslinked P4VP. With increase in 1,4-dibromobutane content, more spherical polymer domains can be observed on the surface of the DX-0 membranes. This behaviour can be attributed to the less molecular interaction between mono quaternized P4VP polymers due to the low degree of crosslinking. Overall, SEM images have demonstrated a uniform distribution of PVC and poly (4-vinyl pyridine) within the membrane matrix.

SEM-EDX analysis was employed to examine the elemental composition of PVC, DX-0 and DX-100 membrane. Br was found in significant weight percentage in DX-0 membrane (Supplementary information, Fig. 1S and Table 1S). Completely crosslinked DX-100 membrane has lost all the Br of 1,4-dibromobutane owing to the bi-functionalization while the least crosslinked DX-0 membrane has retained Br due to mono functionalization. This analysis indicates that a certain ratio of 4-vinyl pyridine and 1,4-dibromobutane is necessary to form membranes with adjustable degree of crosslinking. Since, calculated amount of cross linker is used during membrane synthesis; a quantitative analysis of the degree of crosslinking is not carried out in the synthesized membrane (theoretically estimated degree of crosslinking is shown in Table 1).

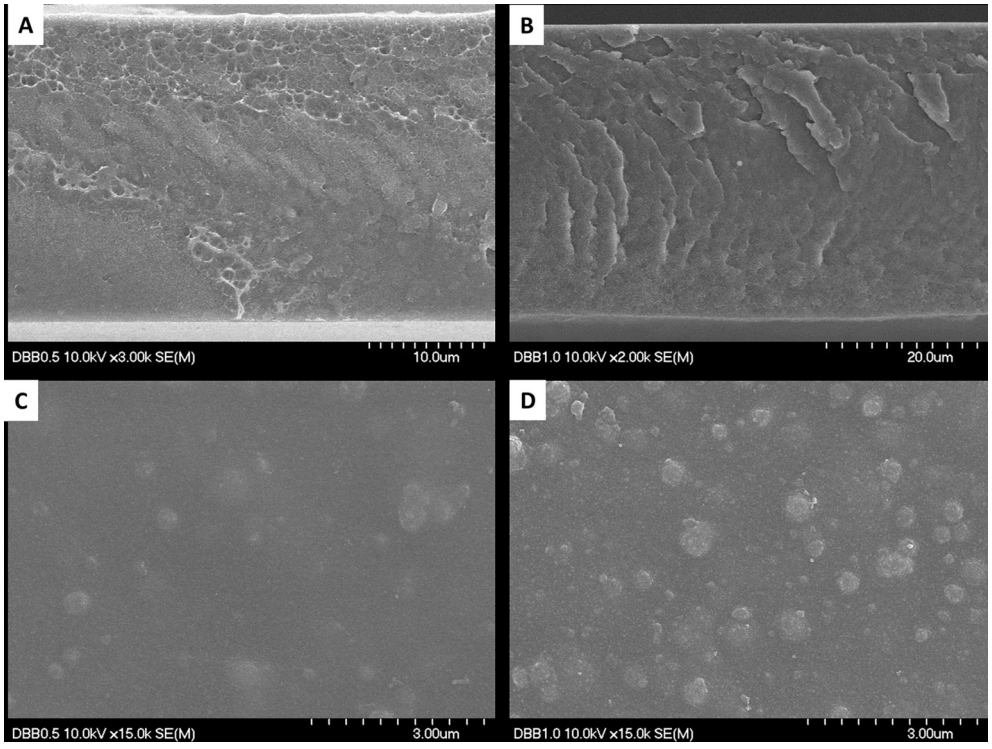

Fig. 3. SEM images of the cross section and surface images of membranes (DX-0 (right) and DX-100 (left)).

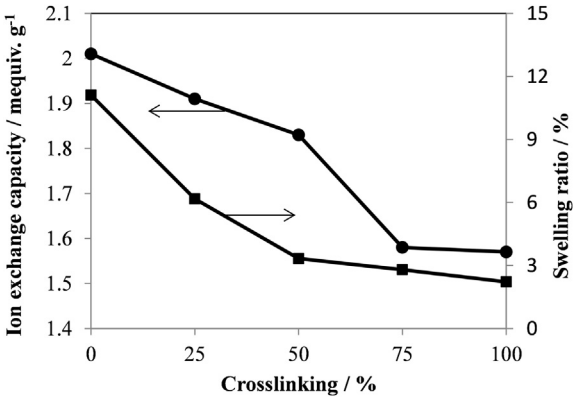

Fig. 4. Influence of the degree of crosslinking on ion exchange capacity and swelling behaviour.

3.2. Ion exchange capacity and swelling ratio

Ion exchange capacity (IEC) is an important factor in determining the performance of AEMs. It provides information on the density of accessible fixed cation sites in the membrane. Fig. 4 shows the results of the IEC measurements and swelling ratio of the AEMs. The prepared membranes showed a superior IEC with a comparable swelling property when compared to Neosepta AHA membrane which has an IEC of 0.95 mequiv. g^{-1} and swelling ratio of 8.6%. Anion exchange sites exist as a pyridinium group and the amount of 4-vinyl pyridine in every membrane was kept equal. In other words, the density of pyridinium group was kept constant for all membranes, though the IEC increased with increase in mole fraction of DBB. The increase in the amount of DBB causes the mono functionalization due to the vast availability of reaction sites and hence decreases the degree of crosslinking. Therefore, DX-0 is minimally crosslinked, DX-100 membrane is fully crosslinked and other membranes placed in between them according to the mole fraction of DBB. The increase in degree of crosslinking causes sluggish ion transport in dense-crosslinked membrane matrix and thus reduces the IEC of the corresponding membrane.

In general, crosslinking is one of the options to improve dimensional stability of the membrane. The synthesized membranes showed excellent dimensional stability due to the interpolymer network of PVC and crosslinked poly(4-vinyl pyridine) chains. Good dimensional stability of membrane is an evidence of advantage of simultaneous polymerization and quaternization which brought crosslinking into membrane matrix at the same time. From Fig. 4 it can be seen that the synthesized membranes

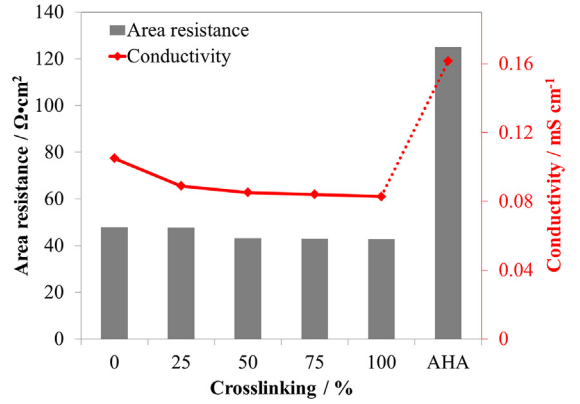

Fig. 5. Influence of DBB mole fraction on conductivity and area resistance.

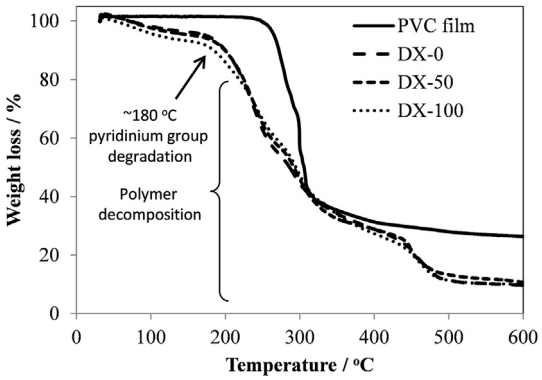

Fig. 6. Thermogravimetric analysis (a) PVC film, (b) DX-0, (c) DX-50, and (d) DX-100.

have a superior swelling ratio than commercial membrane. It can also be observed that the swelling ratio also tends to decrease with the degree of crosslinking which also indicates formation of dense membrane matrix due to crosslinking.

3.3. Membrane electrical resistance and ionic conductivity

The ionic conductivity of the membranes is of particular importance and plays vital role in redox flow battery performance. High resistance of membrane lowers the voltage efficiency and hence overall energy efficiency of the flow cell [27]. The conductivity of tetrafluoroborate ion within the membrane was as a figure of merit for relative conductivity because non-aqueous VRFB uses tetrafluoroborate anion for balancing electroneutrality which gradually replaces chloride ions from the membrane. Fig. 5 presents the electrochemical properties of AEMs in terms of the ionic conductivity and area resistance. As shown in the Fig. 5, the ionic conductivities of the membranes decreased with the increasing crosslinking. The maximum conductivity achieved in our synthesized membrane was 0.105 mS cm^{-1} for the least crosslinked DX-0 and gradually decreases with increase in crosslinking. Overall the ionic conductivity was found to be at least 1 order less compared to conductivities with hydroxide or chloride anion, due to the less mobility of bulky tetrafluoroborate anion than hydroxide or chloride anion [28]. It is well known that the high degree of crosslinking makes polymer chains stiffer therefore the formation of ionic channels is hindered. These undeveloped ionic channels cannot transport ions effectively and therefore ionic conductivity for crosslinked membrane remains lower as the mobility of ions is stalled. Therefore, DX-0 membrane showed higher ionic conductivity for tetrafluoroborate anion when compared to highly crosslinked DX-100 membranes.

Interestingly, the area resistance of synthesized AEMs was found 45 ± 3 Ω cm^2 which is 2.8 times less than commercial Neosepta AHA membrane with 125 Ω·cm^2. High ionic conductivity and low area resistance are crucially important to afford the high voltage efficiency of the redox flow battery [27]. The overall electrochemical properties were superior for the synthesized membranes due to their high ion exchange capacity and low area resistance. Among the synthesized AEMs, DX-0, DX-50 and DX-100 were chosen for further characterization and non-aqueous VRFB single cell test to investigate the effects of crosslinking on the cell performance.

3.4. Stability of the membrane

The thermal stability of PVC, DX-0, DX-50 and DX-100 were evaluated by thermogravimetric analysis (Fig. 6). While PVC

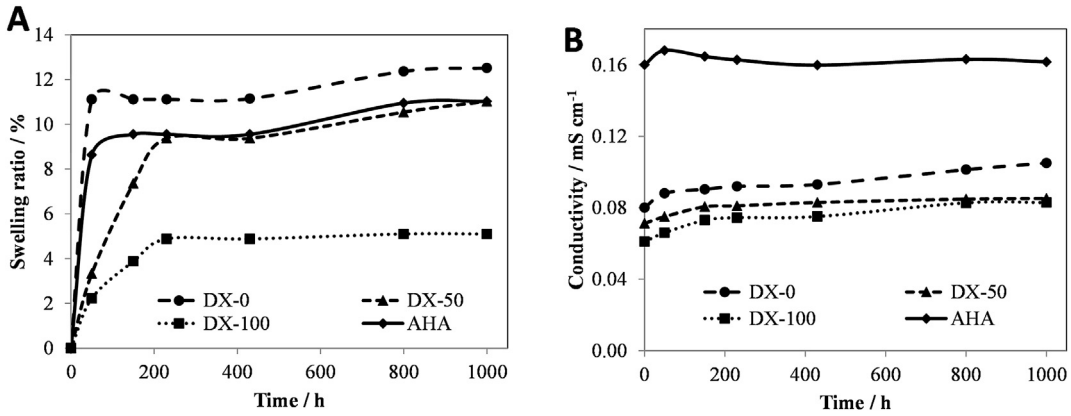

Fig. 7. Change in the membrane properties during exposure of electrolyte solution (A) Change in swelling ratio, and (B) Change in ionic conductivity.

displays only one stage degradation pattern in a 250–350 °C temperature range, all quaternized membranes shows three stage degradation patterns. The first weight loss step (below 100 °C) is due to the removal of existing moisture in the membranes, which is in good agreement with O–H absorption band at 3400 cm^{-1} in FT-IR spectra. The second weight loss step at 180–200 °C is due to the degradation of pyridinium group [29] and the last weight loss over 300 °C was due to the decomposition of polymer backbone that is distinct from neat PVC, and therefore it is a sign of successful polymerization. These results confirm that the pyridinium groups are stable up to 180 °C in transient measurement with no weight loss. However, thermal stability during transient measurement can be different from the actual prolonged exposure. Although the introduction of the pyridinium group by quaternization has decreased the overall thermal stability of the membranes, the AEMs still show good stability below 180 °C, which is similar to other reported AEMs [20].

Non-aqueous VRFB charge/discharge process contains three oxidation states of vanadium i.e., II, III and IV and tetraethylammonium tetrafluoroborate as a supporting electrolyte. Unlike their aqueous counterpart (V (V) and strong acid as supporting electrolyte, highly oxidative chemical surrounding), they operate under relatively mild chemical atmosphere. However, several polymers tend to degrade in acetonitrile and propylene carbonate solution of $TEABF_4$. Electrochemical oxidative degradation of the polymer is the interaction of oxidized polymer with nucleophilic components of the solution. Moreover, use of the organic solvents may dissolve the polymer chains due to existing crystallinity [30], which may result in excessive swelling of the membrane and dissolution of polymer content. Thus, sustained exposure of organic electrolyte-solvent and redox reaction may deteriorate the chemical integrity of polymer chains resulting in decreased dimensional stability. In RFB, the dimensional stability of membranes is also important to assure its mechanical stability as the electrolyte solution flows through the membrane. Thus, the dimensional and chemical stability were assessed in 0.01 M $V(acac)_3$/0.1 M $TEABF_4$/CH_3CN solution by means of swelling ratio and ionic conductivity at room temperature.

The swelling ratio was measured for all membranes by soaking in electrolyte solution and the results were compared with commercial Neosepta AHA membrane (Fig. 7A). The swelling was likely to occur because of wetting of polymer and absorption of the solution. In swelled membrane transport of ions is much easier due to the solvated ionic channels and therefore, ionic conductivity was initially increased with the swelling (Fig. 7B). Furthermore, all the membranes have not shown a more swelling once stabilized over 200 h. As a result, no notable increment in ionic conductivity was observed after 200 h of exposure. Membranes DX-0, DX-50, DX-100 and Neosepta AHA displayed swelling ratio of 12.5%, 11.0%, 5.1% and 11.0% respectively after 1000 h exposure of electrolyte solution. The swelling ability of the polymer membranes was determined by their affinity to the solvent and network elasticity [31]. In particular, all synthesized membranes consist of PVC/quaternized P4VP interpolymer therefore affinity towards solvent remained identical for all membranes. Among the synthesized membranes, the DX-100 membrane has exhibited the lowest swelling, whereas the DX-0 membrane has shown maximum swelling behaviour, which can be attributed to the stiff polymer structure of DX-100 membrane caused by the high degree of crosslinking.

Ionic conductivities of DX-0, DX-50, DX-100 and Neosepta AHA membranes were found to be 0.105, 0.085, 0.083 and 0.162 mS cm^{-1} respectively after exposure of 1000 h, which is a slight improvement in initial conductivity value. It can be attributed to the presence of solvent in the membrane matrix due to the swelling which facilitates the transport of anions. The swelling ratio and ionic conductivity values are in good accordance with the degree of cross-linking. As expected, synthesized membranes have retained the chemical and mechanical integrity during the stability test. Here, it should also be noticed that the interpolymer structure of polyvinyl chloride and poly (4-vinyl pyridine) provides an additional strength against solvent attack since such type of polymer network is known to suppress the swelling and water uptake [32]. Limited swelling was found in all synthesized membranes which assures the mechanical and dimensional stability during long term operation of non-aqueous VRFB.

Table 2
Permeability data of vanadium species through the synthesized membranes.

Membrane	Thickness, μm	Permeability ($\times 10^{-07}$), $cm^2\ s^{-1}$		
		$V(acac)_3^-$	$V(acac)_3$	$V(acac)_3^+$
DX-0	37 ± 2	0.775	1.910	15.50
DX-50	32 ± 4	0.915	2.560	7.090
DX-100	32 ± 4	0.676	1.220	0.930
AHA	200 ± 2	1.990	1.720	1.980

3.5. Vanadium permeability of AEMs

The crossover of vanadium species through a membrane is one of the critical issues which should be resolved to have better RFB performance. Diffusion of charged vanadium species to the opposite chamber leads to self-discharge of a battery i.e., capacity loss without any electrical load between the electrodes. The self-

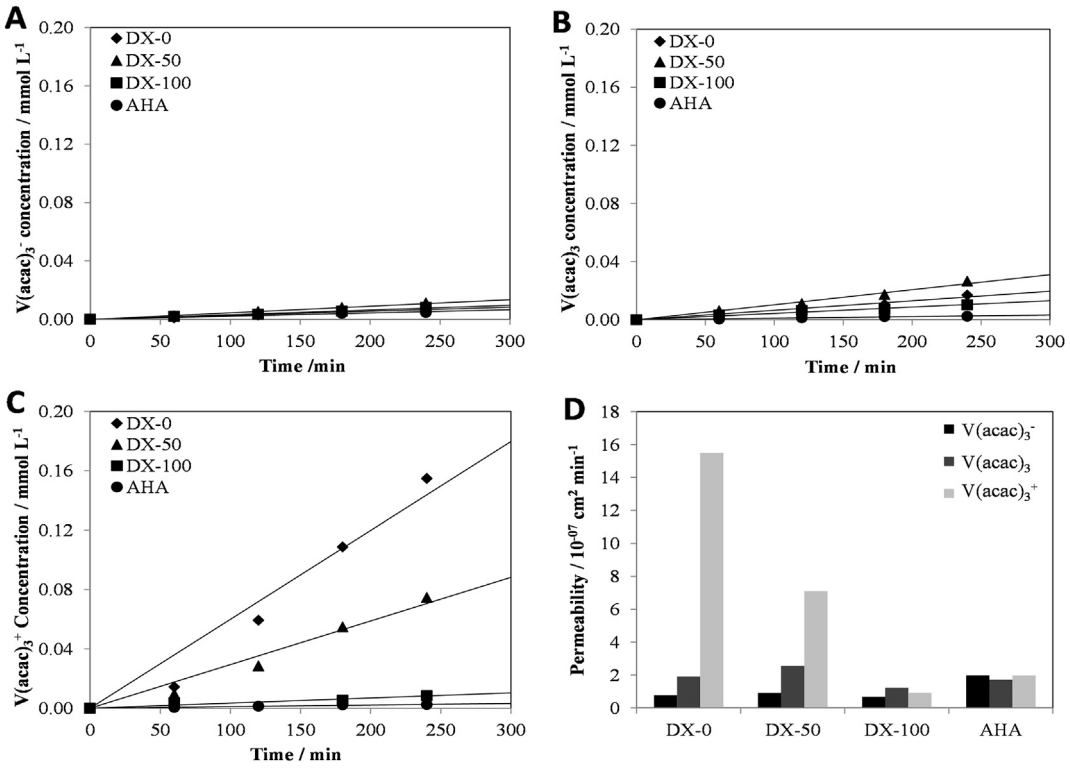

Fig. 8. The permeability of vanadium species Vs. time (A) $V(acac)_3^-$, (B) $V(acac)_3$, (C) $V(acac)_3^+$ and (D) permeability values of membranes.

discharge can be divided into two parts, one is capacity loss by permeation of charged species and other being capacity loss by side reaction of electrolytes with air, moisture, and impurities. The latter effect was minimized by performing the entire testing in the argon filled glove box.

The permeability of vanadium species through the membrane for negative, neutral and positively charged $V(acac)_3$ are summarized with their thickness in Table 2. It is clear from Fig. 8A–D that permeation of vanadium species increases steadily with the time and follows general trend of $V(acac)_3^- < V(acac)_3 < V(acac)_3^+$. The permeation of all charged species found to behave in an equivalent manner with some acceptable deviation in case of DX-100 and Neosepta AHA membranes. In this study, DX-100 and Neosepta AHA membranes has displayed a minimum permeability of active species, among them DX-100 has shown the lowest value (Fig. 8D). Meanwhile, permeability of DX-0 and DX-50 membranes for negatively charged species were found similar to that of DX-100 and Neosepta AHA membranes. Steep increase was observed for neutral and positively charged species in DX-0 and DX-50 membranes. The crossover rate of neutral species for DX-0 and DX-50 membranes were found approximately 1.5 times greater than that of DX-100 and Neosepta AHA membrane. Positively charged species were found to be easily permeated through DX-0 and DX-50 membrane as diffusion rates were 16.6 and 7.6 times higher than that of DX-100 membrane, respectively. The high permeability for DX-0 and DX-50 membrane resulted from the moderate degree of crosslinking as well as the relatively high swelling ratio. The effect of ionic size would be considered because two mutually crosslinked poly(4-vinyl pyridine) chains are separated by ~0.7 nm long linear 4-carbon chain. Therefore, supporting electrolyte anion BF_4^- of 0.55 nm size transported easily while transport of $V(acac)_3$ of 0.9 nm size and charged species were restricted through the crosslinked membrane [21]. Also, ionic size of charged vanadium species follows trend as $V(acac)_3^- > V(acac)_3 > V(acac)_3^+$. Thus, DX-100 showed lowest permeation for charged and neutral vanadium species. DX-0 and DX-50 membrane consist of relatively loose membrane matrix where distance between two poly(4-vinyl pyridine) chain is not limited to 0.7 nm. Therefore such membranes have shown relatively higher permeability according to the ionic size of vanadium species. So far it was thought that positively charged vanadium species poorly diffuses from AEM due to the Donnan exclusion resulted from the anion exchange functional group [22,33]. However, in this study, positively charged species exhibited maximum crossover, it would be attributed to the smallest ionic radius of the positively charged species. Moreover, the poor ionic interaction between anion exchange sites and positively charged species in organic solution declines the possibility for Donnan exclusion.

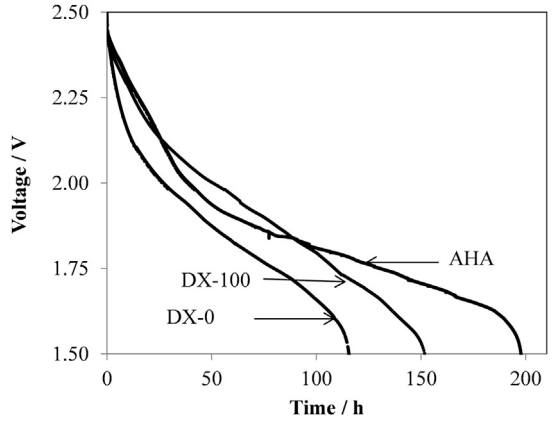

Fig. 9. Open circuit voltage decay of non-aqueous VRFB with DX-0, DX-100 and Neosepta AHA membrane as a function of time.

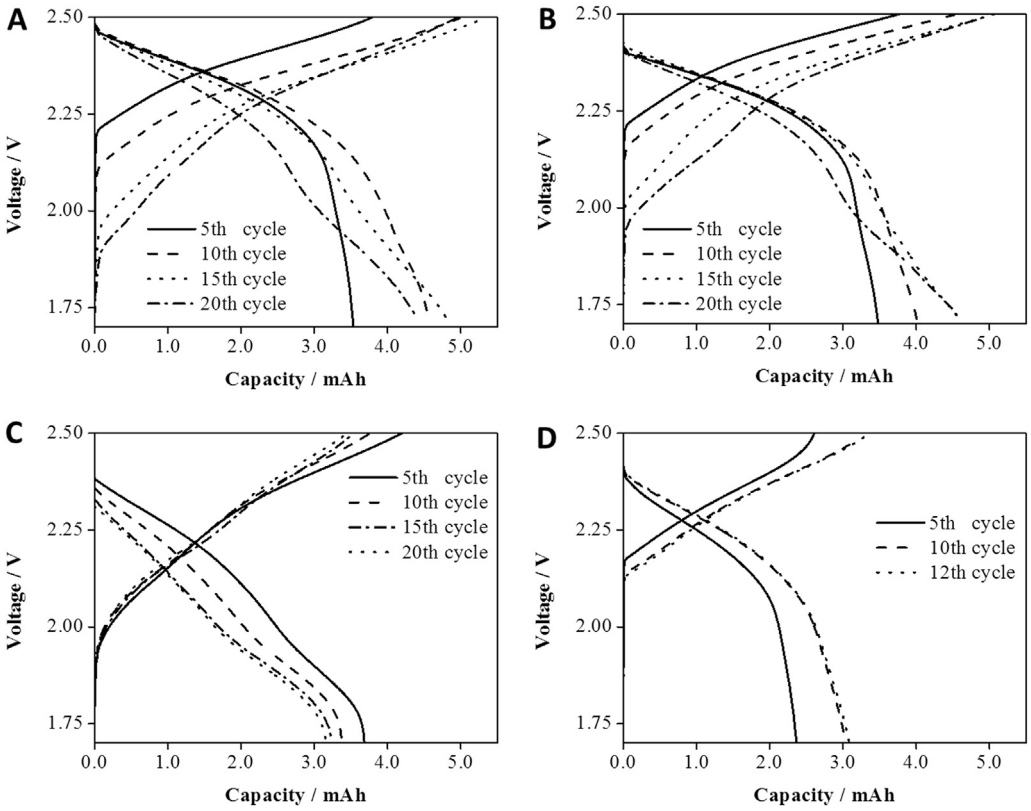

Fig. 10. Charge/discharge curves of non-aqueous VRFB for (A) DX-0, (B) DX-50, (C) DX-100 and (D) Neosepta AHA membranes.

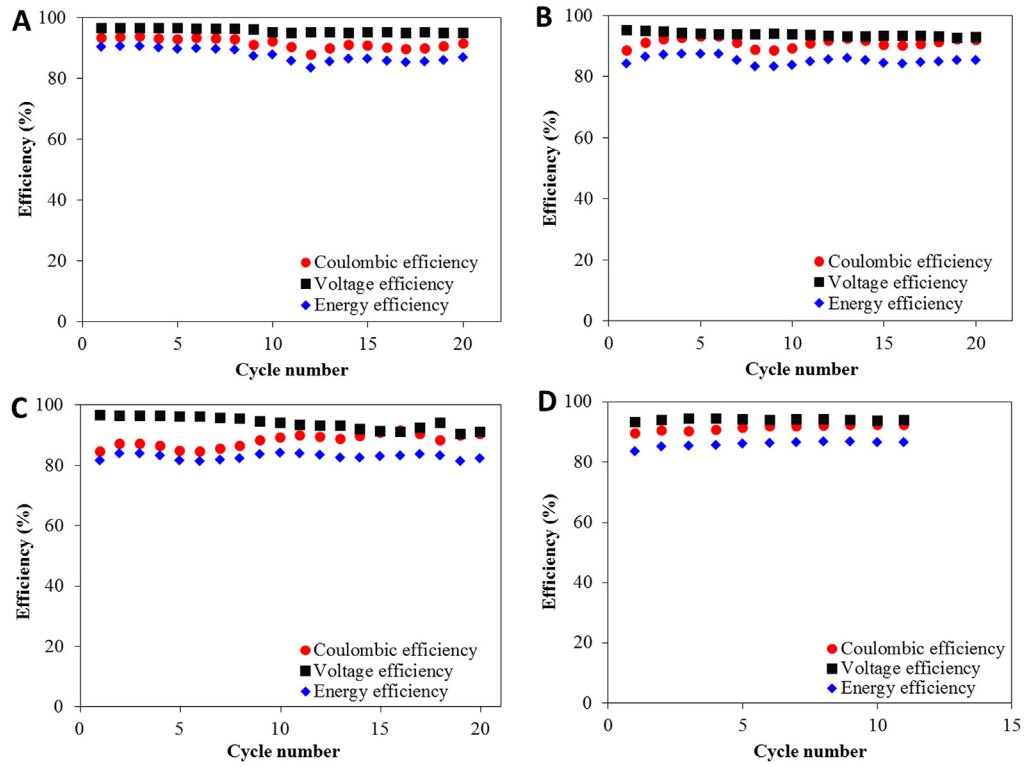

Fig. 11. Efficiencies according to charge/discharge cycles for non-aqueous VRFB (A) DX-0, (B) DX-50, (C) DX-100 and (D) Neosepta AHA membrane.

Table 3
Performance of synthesized AEMs in non-aqueous VRFB.

Membrane	Capacity[a] (mAh)		Efficiency[a], %		
	Charge	Discharge	CE	VE	EE
DX-0	5.0	4.7	91.6	95.7	87.7
DX-50	4.5	4.2	90.0	93.7	85.2
DX-100	3.8	3.4	88.8	91.2	81.0
AHA	2.9[b]	2.6[b]	91.4[b]	94.0[b]	85.9[b]

[a] Average of 20 cycles.
[b] Average of 12 cycles.

Open circuit voltage curves for DX-0, DX-100 and Neosepta AHA membrane are reported in Fig. 9. As expected highly crosslinked DX-100 membrane and thick Neosepta AHA membrane has exhibited slow OCV decay rate which is in accordance with permeability results. DX-0 membrane has displayed fast OCV decay, due to its slack membrane matrix occurred from the least amount of crosslinking.

3.6. A non-aqueous vanadium acetylacetonate redox flow cell test

The applicability and performance of synthesized AEMs for non-aqueous VRFB system were tested in a flow-type RFB cell. The cell was charged up to a voltage of 2.5 V (99.99% state of charge) and then discharged to 1.7 V (0.01% state of charge) at the 0.1 mA cm^{-2} current density. The representative charge and discharge curves are shown in Fig. 10 with the respective capacity. In the discharge curve voltage was initially dropped slightly due to the internal resistance of RFB cell and then stable voltage plateau was observed before 2.0 V after that it fell sharply to the cut-off voltage of 1.7 V due to the mass transport limitation for all the membranes. The second voltage plateau in later cycles has been associated with the formation of vanadyl byproducts [34]. Moreover, the discharge capacities tend to stabilize in early cycles, however, capacity loss was observed in subsequent charge/discharge cycles [34].

DX-0, DX-50, DX-100 and Neosepta AHA membranes achieved average charge/discharge capacity of 5.0/4.7 mAh, 4.5/4.2 mAh, 3.8/3.4 mAh and 2.9/2.6 mAh, respectively (Supplementary information, Fig. 3S). DX-0 attained the maximum average charge and discharge capacity which can be attributed to the comparatively high ionic conductivity aroused from the least degree of crosslinking and high IEC. The average charge/discharge capacity was likely to decrease from DX-0 to DX-100 membranes due to the gradual decrease of the ionic conductivity. Even though the Neosepta AHA membrane holds good ionic conductivity, the charge/discharge capacity was significantly lesser than synthesized membranes due to its 2.8 times higher area resistance than synthesized membrane. The DX-100 and Neosepta AHA membrane displayed slightly lower average charge/discharge capacities while they are least permeable for vanadium species in the non-aqueous electrolyte, which can expand the time period required for electrolyte regeneration. Therefore, these membranes can be more useful for the long term operation.

The CE, VE, and EE with the cycle numbers are shown in Fig. 11 and the average efficiencies of synthesized AEMs are compared with Neosepta AHA membrane in Table 3. It can be seen that efficiencies of synthesized membranes are comparable with Neosepta AHA membrane and especially DX-0 membrane exhibited higher efficiencies in the same experimental condition. The DX-0 membrane has shown maximum permeability for charged vanadium species though; it retains CE, VE and EE of 91.6%, 95.7% and 87.7% which can be attributed to the high IEC, ionic conductivity and smooth transport of supporting electrolyte. It suggests that the high conductivity and optimized microstructure allow enhanced transport of supporting electrolyte together with some active species crossover; subsequently a good non-aqueous VRFB performance was obtained. Interestingly, the energy efficiencies reported in this paper are considerably higher than previous reports because the voltage range (1.7–2.5 V) is carefully chosen according to the state of charge (0.01–99.99%) of the electrolyte [16,20]. Therefore, voltage efficiency was improved to >90% and later, energy efficiency was also improved significantly. Fig. 11 shows that energy efficiencies are retained during the cyclic test which in turn is an evidence for the stability of the synthesized membranes under experimental condition.

In this study, we have applied relatively low charge/discharge current density to avoid local charge/discharge due to low electrolyte concentration (0.01 M $V(acac)_3$ and 0.1 M $TEABF_4$) and restriction for flow rate of electrolyte in a RFB cell. Further studies are on-going to optimize the charge/discharge current density for a non-aqueous VRFB.

4. Conclusion

In this study, a simultaneous polymerization and quaternization method is developed for the synthesis of P4VP-DBB anion exchange membrane where, the monomers are directly polymerized and quaternized by 1,4-dibromobutane in a single step. 1,4-dibromobutane is used to change the crosslinking density of the membrane. This synthetic route has the following advantages: (a) simple, single step and environmentally friendly process, (b) no chloromethylation required for anion exchange functional group and (c) no separate step needed for quaternization. The membrane properties such as ion exchange capacity, ionic conductivity and swelling behaviour are tuned by varying the degree of crosslinking. These AEMs exhibited low vanadium permeability, while retaining good dimensional and chemical stability in an electrolyte solution, making them appropriate candidates for non-aqueous VRFB applications. As observed in the charge/discharge characteristics of non-aqueous VRFB single cell, the capacity and overall efficiency of synthesized AEMs are higher than that of the Neosepta AHA membrane. The energy efficiency of DX-0 membrane is 87.7% which is better than 85.9% efficiency shown by Neosepta AHA membrane under the same experimental condition. Crossover of vanadium species in non-aqueous VRFB is significantly suppressed at a high degree of crosslinking which is advantageous for long term non-aqueous VRFB operation. This study reveals that the non-aqueous VRFB performance is greatly influenced by membrane properties; therefore the optimal control over the membrane properties is advantageous for the improved performance.

Acknowledgement

This work was supported by the National Research Foundation of Korea Grant funded by the Korean Government (MEST) (NRF-2011-C1AAA001-0030538).

Appendix A. Supplementary data

Supplementary data related to this article can be found at http://dx.doi.org/10.1016/j.jpowsour.2014.01.047.

References

[1] E. Sum, M. Rychcik, M. Skyllas-Kazacos, J. Power Sources 16 (1985) 85–95.
[2] E. Sum, M. Skyllas-Kazacos, J. Power Sources 15 (1985) 179–190.
[3] M. Skyllas-Kazacos, M. Rychcik, R.G. Robins, A.G. Fane, J. Electrochem. Soc. 133 (1986) 1057–1058.
[4] M. Skyllas-kazacos, J. Power Sources 35 (1991) 399–404.

[5] S. Peng, N. Wang, C. Gao, Y. Lei, X. Liang, S. Liu, Y. Liu, Int. J. Electrochem. Sci. 7 (2012) 4388–4396.
[6] A.Z. Weber, M.M. Mench, J.P. Meyers, P.N. Ross, J.T. Ghostick, Q. Liu, J. Appl. Electrochem. 41 (2011) 1137–1164.
[7] W. Wang, Q. Luo, B. Li, X. Wei, L. Li, Z. Yang, Adv. Funct. Mater. 23 (2013) 970–986.
[8] X. Wei, Z. Nie, Q. Luo, B. Li, B. Chen, K. Simmons, V. Sprenkle, W. Wang, Adv. Energy Mater. 3 (2013) 1215–1220.
[9] G. Radford, J. Cox, R. Wills, F. Walsh, J. Power Sources 185 (2008) 1499–1504.
[10] H.Q. Zhu, Y.M. Zhang, L. Yue, W.S. Li, G.L. Li, D. Shu, H.Y. Chen, J. Power Sources 184 (2008) 637–640.
[11] L. Yue, W. Li, F. Sun, L. Zhao, L. Xing, Carbon 48 (2010) 3079–3090.
[12] W. Li, J. Liu, C. Yan, Carbon 49 (2011) 3463–3470.
[13] Y. Matsuda, K. Tanaka, M. Okada, Y. Takasu, M. Morita, T. Matsumura-Inoue, J. Appl. Electrochem. 18 (1988) 909–914.
[14] M.H. Chakrabarti, R.A.W. Dryfe, E.P.L. Roberts, Electrochimica Acta 52 (2007) 2189–2195.
[15] W. Wang, W. Xu, L. Cosimbescu, D. Choi, L. Li, Z. Yang, Chem. Commun. 48 (2012) 6669–6671.
[16] Q. Liu, A.E.S. Sleightholme, A.A. Shinkle, Y. Li, L.T. Thompson, Electrochem. Commun. 11 (2009) 2312–2315.
[17] Q. Liu, A.A. Shinkle, Y. Li, C.W. Monroe, L.T. Thompson, A.E.S. Sleightholme, Electrochem. Commun. 12 (2010) 1634–1637.
[18] A.E.S. Sleightholme, A.A. Shinkle, Q. Liu, Y. Li, C.W. Monroe, L.T. Thompson, J. Power Sources 196 (2011) 5742–5745.
[19] C.W. Monroe, A.A. Shinkle, A.E.S. Sleightholme, L.T. Thompson, AIChE Annual Meeting, Salt Lake City, UT, 2010.
[20] S. Maurya, S.-H. Shin, M.-K. Kim, S.-H. Yun, S.-H. Moon, J. Memb. Sci. 443 (2013) 28–35.
[21] S.-H. Shin, S.-H. Yun, S.-H. Moon, RSC Adv. 3 (2013) 9095–9116.
[22] S.-J. Seo, B.-C. Kim, K.-W. Sung, J. Shim, J.-D. Jeon, K.-H. Shin, S.-H. Shin, S.-H. Yun, J.-Y. Lee, S.-H. Moon, J. Memb. Sci. 428 (2013) 17–23.
[23] H. Zhang, H. Zhang, F. Zhang, X. Li, Y. Li, I. Vankelecom, Energy Environ. Sci. 6 (2013) 776–781.
[24] T. Aritomi, T. Isomura, K. Fukuta, K. Sakata, J. Ion Exch. 14 (2003) 193–196.
[25] T. Mohammadi, M. Skyllas Kazacos, J. Power Sources 63 (1996) 179–186.
[26] A. Huang, C. Xiao, L. Zhuang, J. Appl. Polym. Sci. 96 (2005) 2146–2153.
[27] D. Chen, S. Wang, M. Xiao, Y. Meng, J. Power Sources 195 (2010) 2089–2095.
[28] J.A. Vega, C. Chartier, W.E. Mustain, J. Power Sources 195 (2010) 7176–7180.
[29] P. Mondal, S.K. Saha, P. Chowdhury, J. Appl. Polym. Sci. 127 (2013) 5045–5050.
[30] M.A. Hickner, H. Ghassemi, Y.S. Kim, B.R. Einsla, J.E. McGrath, Chem. Rev. 104 (2004) 4587–4611.
[31] J. Ostrowska-Czubenko, M. Pieróg, M. Gierszewska-Drużyńska, Pol. Tow. Chitynowe XVI (2011) 147–157.
[32] S. Kim, S. Park, S. Kim, React. Funct. Polym. 55 (2003) 53–59.
[33] S. Zhang, C. Yin, D. Xing, D. Yang, X. Jian, J. Memb. Sci. 363 (2010) 243–249.
[34] A.A. Shinkle, A.E.S. Sleightholme, L.D. Griffith, L.T. Thompson, C.W. Monroe, J. Power Sources 206 (2012) 490–496.